

Enriched Gradient Recovery for Interface Solutions of the Poisson-Boltzmann Equation

George Borleske, Y. C. Zhou¹

Department of Mathematics, Colorado State University, Fort Collins, CO 80523

Abstract

Accurate calculation of electrostatic potential and gradient on the molecular surface is highly desirable for the continuum and hybrid modeling of large scale deformation of biomolecules in solvent. In this article a new numerical method is proposed to calculate these quantities on the dielectric interface from the numerical solutions of the Poisson-Boltzmann equation. Our method reconstructs a potential field locally in the least square sense on the polynomial basis enriched with Green's functions, the latter characterize the Coulomb potential induced by charges near the position of reconstruction. This enrichment resembles the decomposition of electrostatic potential into singular Coulomb component and the regular reaction field in the Generalized Born methods. Numerical experiments demonstrate that the enrichment recovery produces drastically more accurate and stable potential gradients on molecular surfaces compared to classical recovery techniques.

Keywords: Biomolecular electrostatics; Poisson-Boltzmann equation; Numerical Solution; Interface methods; Gradient recovery; High accuracy
2014 MSC: 53B10, 65D18, 92C15

1. Introduction

The Poisson-Boltzmann theory has been widely accepted as a mean-field continuum approximation for electrostatic interactions in solvated biomolecular systems [1]. The Poisson-Boltzmann theory treats the solute biomolecules as a singularly charged medium of low dielectric constant ($\epsilon_p = 1 \sim 2$) immersed in a high dielectric ($\epsilon_s = 75 \sim 80$) solvent with a continuum charge

¹Corresponding author. Email: yzhou@math.colostate.edu

distribution that models the dispersed mobile ions. The large contrast of dielectric constant on the highly complicated biomolecular surfaces poses a significant computational challenge and affords delicate mathematical and numerical treatments. The importance of Poisson-Boltzmann theory in biochemistry and biophysics has motivated extensive mathematical and computational investigations, see, for instance [2, 3, 4, 5, 6, 7], and references therein for the development of the subjects in the past decades and the latest overviews.

This paper is concerned with the accurate calculation of the gradient of the electrostatic potential $\nabla\phi$ near the molecular surface from the numerical solutions of the Poisson-Boltzmann equation (PBE) for modeling solvated biomolecules. Traditionally the potential solutions of the Poisson-Boltzmann equation are used merely for computing the solvation free energy (and other derived energetic quantities such as pKa value, binding affinity, etc.), and therefore less attention had been paid on the calculation of the potential gradient. The success of Poisson-Boltzmann theory in these energetic evaluations promotes the exploration of PBE based electrostatic force calculations for molecular dynamics (MD) simulations [8, 9, 10, 11] and coarse-grained [12, 13] or hybrid models [14, 15, 16]. There are three types of electrostatic forces defined by using the free energy functional derivatives and shape derivatives [17, 18, 19, 20], including (i) the body force exerted at each charged atoms of the solution molecules given by $qE = q\nabla\phi$ where q is the local charge density; (ii) the dielectric boundary force exerted on the dielectric interface that is usually defined by the molecular surface; and (iii) the ionic pressure, exerted also on the molecular surface.

Perpendicular to the dielectric interface, the dielectric boundary force

$$f_n = -\frac{\epsilon_s}{2}|\nabla\phi^s|^2 + \frac{\epsilon_p}{2}|\nabla\phi^p|^2 - \epsilon_p|\nabla_n\phi^p|^2 + \epsilon_p(\nabla_n\phi^s)(\nabla_n\phi^p) \quad (1)$$

poses significant challenges to the numerical computation because it is defined on the dielectric interface where one usually observes the peaks of the numerical error in the solutions of the Poisson-Boltzmann equation [21, 22, 23, 24, 25, 26, 27, 28]. For boundary element methods, while $\nabla_n\phi^s$ can be obtained directly along with ϕ^s from well-conditioned boundary integral formulations, computing $\nabla\phi^p$ involves additional integrations of the numerical solution of the potential with a supersingular kernel over the entire surface [29, 30, 31, 7], usually causing a larger error. For finite difference interface methods, one usually extrapolates the potential solution across the interface

by using the interface conditions to compute potential gradients [11]. For interface finite elements methods, gradient recovery techniques are recently developed so that potential gradient could be computed in a subdomain without using the solution values across the internal interface [32, 33, 34].

We will develop an interface gradient recovery method to approximate the screened electrostatic potential from the numerical solution of the Poisson-Boltzmann equation. For elliptic problems with smooth coefficients, gradient recovery techniques have been well established on structured or unstructured grids [35, 36, 37, 38, 39, 40, 41]. By comparison, there is only a small handful of numerical techniques concerning the gradient recovery from the primarily computed solutions of the elliptic problems with piecewise smooth coefficients or singular sources. For 1-D interface problems, special interpolation formulas are constructed to recover flux with high order accuracy from numerical solutions of linear and quadratic interface finite element methods [42, 43]. For 2-D elliptic interface problems on a specially constructed body-fitted mesh, gradient of the linear finite element solution is shown to be superclose to the gradient of the linear interpolation of the exact solution [44]. By introducing the jump in the normal derivative as an augmented variable, Li *et. al.* showed that a second-order convergence can be obtained for the solution and its gradient [45]. Recently developed gradient recovery methods for interface problems are based on the second-order least square reconstruction of the solutions in an individual subdomain [32]. If the mesh is not conforming to the interface, a practice common in many immersed finite element methods [46, 47, 48, 49], the solutions on the interface are first obtained on appropriately subdivided interface elements then supplied to the least square reconstruction [33]. When Nitsche’s method [50, 51] is used for solving the elliptic interface problems, this subdivision of the interface element is not necessary, and one can use the solution on the extended fictitious subdomain to carry out the least square reconstruction [34]. Nevertheless, as we shall demonstrate below, these interface gradient recovery methods are not able to accurately compute the interface potential gradient on a spatial (domain or surface) discretization that are affordable for realistic biomolecular simulations.

Our method is based on the least square reconstruction of the numerical solution, with the classical polynomial basis supplemented with $\{1/r_i\}$ where r_i is the distance between a mesh node and the selected charges in the solute biomolecule. These additional functions have been indicated in the Green’s function for the Poisson equation and particularly in the generalized

Born (GB) models for the biomolecular electrostatics. In GB models, the electrostatics potential at a charge q_i inside the dielectric boundary is given by

$$\phi(x_i) = \sum_{j \neq i} \frac{q_i q_j}{\epsilon_p |x_i - x_j|} + \mathbf{F}(x_i, x_j) \quad (2)$$

where q_i is the singular charge at spatial position \mathbf{x}_i , and \mathbf{F} is the reaction field due to the polarization charges induced at the dielectric boundary [52, 53]. A large variety of GB models have been developed to implicitly account for the effects of solvation through various parameterizations of effective Born radius, solvation accessible surfaces, ionic screening, among others, see [54] for a latest review and references therein. In the solvent domain Ω_s , although an analytical approximation similar to (2) does not exist, the approximation

$$\phi(x) = \sum_i \frac{q_i}{\epsilon_s |x - x_i|} e^{-\kappa |x - x_i|} \quad (3)$$

is widely used to compute the boundary conditions for the Poisson-Boltzmann at a boundary point \mathbf{x} far away from the solute molecules, where κ is the Debye-Huckel inverse screening length. The approximations (2)-(3) motivate us to choose functions of the form $1/r$ to enrich the classical polynomial basis function in the least square reconstruction. Numerical experiments demonstrate that our enriched recovery technique is highly accurate and stable for complicated biomolecules. By construction our recovery technique can be integrated with general interface numerical methods for the Poisson-Boltzmann equation, regardless of whether the discretization mesh is interface conforming or not.

The rest of the article is organized as follows. In Section 2.1, the Poisson-Boltzmann equation and its numerical treatment are briefly reviewed, followed by the introduction of dielectric boundary force and its calculation. We will present the our gradient recovery technique in Section 3 and discuss its extension to enforcing the interface conditions. Extensive numerical experiments will be conducted in Section 4 to verify the robustness and accuracy of our methods on biomolecules of different complexity. The article concludes with a summary in Section 5.

2. Poisson-Boltzmann Equation and Dielectric Boundary Force

This section presents the energetic theory of biomolecular electrostatics. The electrostatic free energy introduced by Sharp, Honig, Gilson *et. al.*

[17, 55, 56, 57] provides a unified theory to connect the electrostatic solvation energy and the Poisson-Boltzmann equation. The inconsistency between their definition of the electrostatic force and the sharp dielectric interface model was recently reconciled through the introduction of a shape derivative of the solute biomolecules and the application of the Hadamard-Zolésio structure theorem [19, 20]. We will review the regularization techniques for the numerical solution of the PBE, which also sheds light to our choice of the enriching basis functions in the least square reconstruction for the gradient recovery.

2.1. Biomolecular electrostatics theory and the Poisson-Boltzmann equation

Consider $\Omega \in \mathbb{R}^3$ be a domain that encapsulates the solute biomolecules and the aqueous solution in which M species of mobile ions disperse. The occupation domains of solute and solvent are respectively denoted by Ω_p and Ω_s , with distinct dielectric constants ϵ_p and ϵ_s . Denote by Γ the dielectric interface separating these two subdomains. Assume dispersion of mobile ions follows the Boltzmann distribution, then the electrostatic free energy of this solvated system is given by

$$G(\Gamma; \phi) = \int_{\Omega} \left[-\frac{\epsilon}{2} |\nabla \phi|^2 + f\phi - \chi_s \beta^{-1} \sum_{j=1}^M c_j^0 (e^{-\beta q_j \phi} - 1) \right] dx, \quad (4)$$

where c_j^0 is the bulk concentration of j^{th} species of ions, $f = \sum_{i=1}^N q_i$ is the collection of singular charges of biomolecule atoms, and $\beta = 1/(k_B T)$ is the inverse thermal energy at temperature T . The characteristic function $\chi_s = 1$ in Ω_s and vanishes elsewhere. Equation (4) highlights the dependence of the electrostatic free energy on the location of the dielectric interface Γ . Minimization of G with respect to ϕ leads to the nonlinear Poisson-Boltzmann equation

$$-\nabla \cdot (\epsilon \nabla \phi) + \chi_s \sum_{j=1}^M c_j^0 q_j e^{-\beta q_j \phi} = \sum_{i=1}^N q_i \delta(x_i), \quad (5)$$

with interface conditions on Γ :

$$[\phi(x)] = 0, \quad [\epsilon \nabla_n \phi] = 0, \quad (6)$$

where $[\cdot]$ denotes the jump of the enclosed function and ∇_n is the normal derivative pointing to Ω_s .

To derive the dielectric boundary force we introduce a surface transformation T_t corresponding to the slight change of domain Ω_p due to the motion of interface Γ in its normal direction. The dielectric boundary force is derived by taking the variational derivative of the free energy G with respect to a velocity field V normal to Γ . Associated with this velocity fields is a mapping $T_t(X)$ from the original surface coordinate $X \in \Gamma_0$ (material position) to the deformed coordinate $x \in \Gamma_t$ (physical position):

$$T_t(X) = x(t, X) = x(0, X) + t \left. \frac{\partial x(t, X)}{\partial t} \right|_{t=0} + \mathcal{O}(t^2). \quad (7)$$

Introducing the Jacobian J_s of the surface transformation T_t :

$$J_s = \det(\nabla T_t(X)) \cdot |\nabla T_t^{-T} \cdot n(X)|, \quad (8)$$

one can show that

$$\nabla \cdot V = \left. \frac{dJ_s}{dt} \right|_{t=0}, \quad (9)$$

and the shape derivative of G

$$\delta_\Gamma G(\Gamma; \phi) = \lim_{t \rightarrow 0} \frac{G(\Gamma_t; \phi) - G(\Gamma_0; \phi)}{t} = \int_{\Gamma_0} -f_n V \cdot n ds, \quad (10)$$

where f_n is the dielectric boundary force given in (1) [20].

Numerical techniques for the PBE are mostly focused on the treatment of the discontinuous dielectric function ϵ and the singular charge density $q_i \delta(x_i)$. There are three major regularization schemes with which a direct approximation of the singular delta functions can be avoided:

(I) Subtract the potential

$$\phi^s(x) = \sum_{i=1}^N \frac{q_i}{\epsilon_s |x - x_i|} \quad (11)$$

induced by the collection of singular charges from the potential in the entire domain Ω , and thus one only needs to numerically solve the remaining regular potential $\phi^r = \phi - \phi^s$ [58]. In solvent domain Ω_s , this potential is much larger than the true potential $\phi = \phi^s + \phi^r$, so is the regular potential ϕ^r there. Consequently a small relative error in the numerical solution of ϕ^r will present a larger relative error in ϕ , constituting an unstable numerical algorithm [59].

- (II) Subtract the singular potential (11) only in the solute domain Ω_p . This will create additional jumps in the remaining regular components. Therefore a harmonic potential ϕ^h defined by

$$\epsilon_p \Delta u^h = 0, \quad x \in \Omega_p; \quad u^h(x) = -\phi^s, \quad x \in \Gamma, \quad (12)$$

is added back to partially compensate the jump and to maintain C^0 continuity of the remaining regular potential at the interface Γ [60]. This strategy greatly improves the stability of the numerical method. On the other hand, one needs to compute $\nabla_n \phi^h$ on Γ to supply the interface conditions for ϕ^r :

$$[\phi^r(x)] = 0, \quad [\epsilon \nabla_n \phi^r] = \epsilon_p \nabla_n \phi^h. \quad (13)$$

Numerical evaluation of $\partial \phi^r / \partial n$ is nontrivial, and might introduce considerable error to the interface condition for ϕ^r . A numerical Dirichlet-Neumann mapping based on boundary integral formulations will make this calculation accurate and efficient [61].

- (III) One could choose not to add back the harmonic potential ϕ^h so there are only two components in the solute domain. The absence of this harmonic component leads to the jumps in the potential and its normal derivative on the dielectric interface

$$[\phi^r(x)] = \phi^s(x), \quad [\epsilon \nabla_n \phi^r] = \epsilon_p \nabla_n \phi^s. \quad (14)$$

On the other hand, this regularization scheme helps reduce the complexity and improve the accuracy as one does not need to supply a numerical computed $\nabla_n \phi^h$ to the related interface condition for the regularized Poisson-Boltzmann equation [28].

Our enriched gradient recovery method is compatible with all these regularization schemes. We shall present the gradient recovery and force calculation along with the following general form of interface conditions:

$$[\phi^r(x)] = g(x), \quad [\epsilon \nabla_n \phi^r] = h(x), \quad (15)$$

with known jumps $g(x), h(x)$.

2.2. Dielectric boundary force and its calculation

To get the dielectric boundary force f_n , one shall first compute ϕ_s, ϕ_p and their respective gradients at selected positions (the centroids of surface triangles, for example) on the interface Γ . There are three different procedures to complete this calculation:

- (I) Independently compute ϕ_s, ϕ_p and their gradients using proper gradient recovery techniques.
- (II) Compute only one set of $(\phi_p, \nabla\phi_p)$ or $(\phi_s, \nabla\phi_s)$, and use the interface conditions (15) to get the other.
- (III) Compute both sets of $(\phi_p, \nabla\phi_p)$ and $(\phi_s, \nabla\phi_s)$ by enforcing the interface conditions (15) in the gradient recovery.

Procedure I is inferior to the others because the resulting dielectric boundary force is not consistent with the interface conditions. Procedures II and III will be developed in Section 3 and implemented in Section 4

3. Gradient Recovery Techniques Enriched with Green's Functions

Our gradient recovery techniques for PBE are based on the least square reconstruction of the numerical solution, which is also the basis of polynomial preserving recovery (PPR) techniques [39, 41] and their recent variations for elliptic interface problems [33, 32, 34]. In this section we will first summarize the standard PPR method and then present its enrichment with Green's functions. This enriched gradient recovery technique will be integrated with different regularization schemes described in Section 2 to enforce the respective interface conditions.

3.1. Polynomial preserving recovery and enrichment with Green's functions

We consider the molecular surface discretized by triangles and assume that the electrostatic potential ϕ has been solved from the Poisson-Boltzmann equation using a finite difference or finite element interface method. The mesh for the interface method may not be fitting the interface triangulation. The electrostatic force is usually computed at the centroids of triangles which are not necessarily the mesh nodes. Our method can be used to calculate the solution derivatives at vertices of surface triangles but one needs a delicate definition of the normal directions at the corner vertices to finally compute the surface force. For a centroid o with coordinate $\mathbf{x}_o = (x_o, y_o, z_o)$ we define

$\mathcal{N}(o, n)$ be the collection of n mesh nodes in solvent domain that are closest to o :

$$\mathcal{N}_s(o, n) = \{v : v \in V_s, |\mathbf{x}_v - \mathbf{x}_o| \leq |\mathbf{x}_z - \mathbf{x}_o| \quad \forall z \notin \mathcal{N}_s(o, n)\}, \quad (16)$$

where V_s are the mesh nodes in Ω_s or on the molecular surface Γ . The numerical solution at this collection of nodes will be fitted by a polynomial $p_s \in \mathbb{P}_k$ in the least square sense sampled at these nodes:

$$p_s(x) = \arg \min_{p \in \mathbb{P}_k} \sum_{v \in \mathcal{N}_s(o, n)} (\phi_s - p)^2(v). \quad (17)$$

We then define the recovered gradient at surface position o as

$$G_o(\phi_s) = \nabla p_s(o). \quad (18)$$

Alternatively, one can choose the collection of nodes in the solute domain Ω_p to fit a polynomial $p_p(x)$ and to compute the recovered gradient

$$G_o(\phi_p) = \nabla p_p(o). \quad (19)$$

As in most analysis and applications of PPR, we choose \mathbb{P}_k to be the space of quadratical polynomials, i.e., $k = 2$.

Remark 1. *The choice of sampling nodes (16) is for general interface methods. For finite element interface methods one can take advantage of mesh structure to choose the mesh nodes in the first l layers around the point o .*

As we will demonstrated in Section 4, the polynomial preserving recovery technique is not able to deliver an accurate surface gradient on grid sizes affordable to practical biomolecular simulations, mostly because polynomial approximation of singular potential components have large truncation errors. Since these singular components are induced by charges at known positions, we will introduce the Green's function as basis functions in addition to the quadratical polynomials in the least square reconstruction, c.f. Fig. 1. **We anticipate that the singular component of the solution will be approximated by these enriching basis functions, while the regular component of the solution will be approximated in the original polynomial space.** For the surface point o given above, we shall choose m charged atoms of the solute molecule that are closest to o :

$$\mathcal{A}_1(o, m) = \{a : a \in \mathcal{A}_p, |\mathbf{y}_a - \mathbf{x}_o| \leq |\mathbf{y}_b - \mathbf{x}_o| \quad \forall b \notin \mathcal{A}_1(o, m)\}, \quad (20)$$

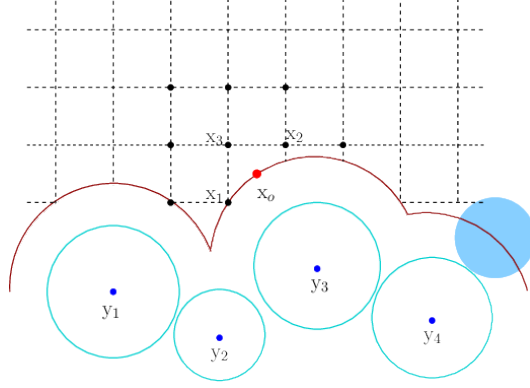


Figure 1: 2-D illustration of polynomial preserving recovery (PPR) and enriched gradient recovery at a surface point \mathbf{x}_o for the interface solution of the Poisson-Boltzmann equation on a Cartesian grid. PPR locally reconstructs solution using a polynomial in the least square sense at selected nodes \mathbf{x}_i (black dots) in the solvent region Ω_s (meshed). Enriched recovery adds Green's functions induced by the charges q_j at the centers \mathbf{y}_j of selected atoms to the polynomial basis. The solvent accessible surface (SAS; red) is chosen to the dielectric interface. SAS is the trace of the center of probe sphere (blue) modeling water molecule as it rolls over the atoms (surface in cyan) of the solute molecule.

where \mathcal{A}_p is the set of all charged atoms of the solute molecule. Alternatively, one may choose all charged atoms within a pre-determined distance r_c to o :

$$\mathcal{A}_2(o, m) = \{a : a \in \mathcal{A}_p, |\mathbf{y}_a - \mathbf{x}_o| \leq r_c\}. \quad (21)$$

Since the singular components decay like $1/r$, contributions to the potential and force from charged atoms far away from o are secondary, and can be well approximated in the original polynomial space. By enriching the polynomial basis of degree 2 with Green's functions centered at a total of m selected charged atoms we define a new space of functions

$$\mathbb{Q}_2 = \text{span} \left\{ 1, x, y, z, x^2, y^2, z^2, xy, yz, xz, \frac{1}{|r_1|}, \dots, \frac{1}{|r_m|} \right\} \quad (22)$$

where x, y, z are the Cartesian coordinates with respect to o and r_m is the distance to m^{th} selected charge. We then fit the numerical solution at mesh nodes in $\mathcal{N}_s(o, n)$ with a function $q_s \in \mathbb{Q}_2$ such that

$$q_s(x) = \arg \min_{q \in \mathbb{Q}_2} \sum_{v \in \mathcal{N}_s(o, n)} (\phi_s - q)^2(v). \quad (23)$$

This amounts to a least square solution $A\mathbf{v} = \mathbf{b}$ where each row of matrix $A \in \mathbb{R}^{n \times (10+m)}$ is corresponding to a sampling mesh node in Ω_s with coordinate (x, y, z) and is given by

$$A_{i,1:10} = (1, \Delta x_i, \Delta y_i, \Delta z_i, \Delta x_i^2, \Delta y_i^2, \Delta z_i^2, \Delta x_i \Delta y_i, \Delta y_i \Delta z_i, \Delta x_i \Delta z_i), \quad (24)$$

$$A_{i,11:10+m} = \left(\frac{1}{|\mathbf{x}_i - \mathbf{y}_1|}, \dots, \frac{1}{|\mathbf{x}_i - \mathbf{y}_m|} \right), \quad (25)$$

where $\Delta x_i = x_i - x_o$, $\Delta y_i = y_i - y_o$, $\Delta z_i = z_i - z_o$ and \mathbf{y}_m is the position of the m^{th} selected charge. Since the functions in (25) are linearly independent with each other and with the polynomial basis in (24), the least square problem (23) is solvable.

Remark 2. *The potential in Ω_s does not have a decomposition with an analytical reaction field $\mathbf{F}(x, x_i)$ similar to (2). However, the approximate solution (3) suggests that it is possible to define a component of the form $1/r$. The space \mathbb{Q}_2 is constructed to approximate this component using $1/r_i$ and the remaining component using the regular polynomial basis.*

Remark 3. *The derivative of the Green's function can also be written in terms of the same Green's function. Thus the derivative of the basis functions in \mathbb{Q}_2 is also in \mathbb{Q}_2 , allowing us to approximate both the potential and its derivatives in the same space.*

Remark 4. *The approximation of the electrostatic potential in \mathbb{Q}_2 for the Born ion [62] is exact.*

3.2. Coupled gradient recovery with interface condition enforcement

We need potentials and potential gradients on both sides of the dielectric interface to compute the dielectric boundary force. These quantities independently recovered on either side using the method described above do not satisfy the interface conditions, although these conditions have been enforced in the interface methods for the numerical solution of the PBE. Procedure II (c.f. Section (2.2)) recovers the solution on one side and generate the surface potential and surface gradient on the other side using the interface conditions. This requires only one least square solution for the gradient recovery at an interface point o , and thus is simpler to implement. It is worth noting that if one chooses to compute $(\phi_p, \nabla \phi_p)$ instead of $(\phi_s, \nabla \phi_s)$, then

the enrichment using Green's function is not necessary, because the singular potential component has been removed from Ω_p in all three regularization schemes here. Coupled gradient recovery on both sides of the interface is also possible by enforcing the interface conditions in least square reconstruction. To this end we shall define in addition to $\mathcal{N}_s(o, n)$ another collection of n mesh nodes in the solute domain, $\mathcal{N}_p(o, n)$, that are closest to o :

$$\mathcal{N}_p(o, n) = \{v : v \in V_p, |\mathbf{x}_v - \mathbf{x}_o| \leq |\mathbf{x}_z - \mathbf{x}_o| \quad \forall z \notin \mathcal{N}_p(o, n)\}. \quad (26)$$

Two functions, one polynomial $p_p \in \mathbb{P}_2$ and the other $q_s \in \mathbb{Q}_2$, respectively sampled on $\mathcal{N}_p(o, n)$ and $\mathcal{N}_s(o, n)$, will be sought from the following problem:

$$(p_p(x), q_s(x)) = \arg \min_{p \in \mathbb{P}_2, q \in \mathbb{Q}_2} \left[\sum_{v \in \mathcal{N}_p(o, n)} (\phi_p - p)^2(v) + \sum_{u \in \mathcal{N}_s(o, n)} (\phi_s - q)^2(u) \right], \quad (27)$$

subject to the interface conditions:

$$q_s(o) - p_p(o) = g(o), \quad \epsilon_s \nabla_n q_s(o) - \epsilon_p \nabla_n p_p(o) = h(o). \quad (28)$$

The solution of (27) leads to a least square problem $A\mathbf{v} = \mathbf{b}$ where the matrix $A \in \mathbb{R}^{(2n+2) \times (20+m)}$ whose first n rows correspond to the approximation of the solution ϕ_p respectively at n sampling nodes (x_i^p, y_i^p, z_i^p) in Ω_p , i.e.,

$$A_{i,1:10} = (1, \Delta x_i^p, \Delta y_i^p, \Delta z_i^p, (\Delta x_i^p)^2, (\Delta y_i^p)^2, (\Delta z_i^p)^2, \Delta x_i^p \Delta y_i^p, \Delta y_i^p \Delta z_i^p, \Delta x_i^p \Delta z_i^p), \quad (29)$$

$$A_{i,11:20+m} = (0, \dots, 0), \quad (30)$$

for $1 \leq i \leq n$. The next n rows of A are for the approximation at sampling nodes (x_i^s, y_i^s, z_i^s) in Ω_s , i.e.,

$$A_{n+i,1:10} = (0, \dots, 0), \quad (31)$$

$$A_{n+i,11:20} = (1, \Delta x_i^s, \Delta y_i^s, \Delta z_i^s, (\Delta x_i^s)^2, (\Delta y_i^s)^2, (\Delta z_i^s)^2, \Delta x_i^s \Delta y_i^s, \Delta y_i^s \Delta z_i^s, \Delta x_i^s \Delta z_i^s), \quad (32)$$

$$A_{n+i,21:20+m} = \left(\frac{1}{|\mathbf{x}_i - \mathbf{y}_1|}, \dots, \frac{1}{|\mathbf{x}_i - \mathbf{y}_m|} \right), \quad (33)$$

for $1 \leq i \leq n$. The last two rows of A come from the approximation of the interface conditions (28):

$$A_{2n+1,1} = -1, \quad (34)$$

$$A_{2n+1,11} = 1, \quad (35)$$

$$A_{2n-1,(2:10,12:20)} = (0, \dots, 0), \quad (36)$$

$$A_{2n+1,21:20+m} = \left(\frac{1}{|\mathbf{x}_o - \mathbf{y}_1|}, \dots, \frac{1}{|\mathbf{x}_o - \mathbf{y}_m|} \right). \quad (37)$$

$$A_{2n+2,(1,5:10,11,15:20)} = (0, \dots, 0), \quad (38)$$

$$A_{2n+2,2:4} = -\epsilon_p(n_x, n_y, n_z), \quad (39)$$

$$A_{2n+2,12:14} = \epsilon_s(n_x, n_y, n_z), \quad (40)$$

$$A_{2n+2,21:20+m} = \epsilon_s \left(\frac{(\mathbf{x}_o - \mathbf{y}_1) \cdot \mathbf{n}}{|\mathbf{x}_o - \mathbf{y}_1|^3}, \dots, \frac{(\mathbf{x}_o - \mathbf{y}_m) \cdot \mathbf{n}}{|\mathbf{x}_o - \mathbf{y}_m|^3} \right). \quad (41)$$

where $\mathbf{n} = (n_x, n_y, n_z)$ is the unit outer normal on the interface. Solution of this least square problem reconstructs functions that approximate the potential solutions at sampling mesh nodes on two sides of the interface and the jump conditions at the interface point o .

4. Numerical Experiments

In this section we validate the accuracy and stability of our enriched gradient recovery method on a set of biomolecules. Since there do not exist exact solutions of the electrostatic surface potential and gradient for general molecules with complex surface geometries, we make up potential fields for accuracy validation of Procedure II by setting the potential in the solvent domain Ω_s to be

$$\phi_s(\mathbf{x}) = \sum_{i=1}^N \frac{q_i}{\epsilon_s |\mathbf{x} - \mathbf{y}_i|}, \quad (42)$$

following the approximation boundary condition (3). The exponential screen term is neglected because the ion strength κ is always small and makes very slight changes to the surface potential and gradient. Procedure II will be used in enriched recovery with analytical fields. We will compare the classical polynomial preserving (PPR) and enriched gradient recoveries on molecules with the potential field (42). We will further solve the Poisson-Boltzmann equation with an interface finite difference method MIB [63, 64], and use the

solution at a fine mesh as the reference to check the accuracy of both PPR and our enriched gradient recoveries. Procedure III will be used since we have solutions available on both sides of the interface. We will use the following absolute and relative errors for quantifying the accuracy of recovered surface potential $R(\phi)$, gradient $R(\nabla_n \phi)$, and force $R(f_n)$ on the interface:

$$e(\phi) = \|R(\phi) - \phi\|_{0,\Gamma}, e(\nabla_n \phi) = \|R(\nabla_n \phi) - \nabla_n \phi\|_{0,\Gamma}, e(f_n) = \|R(f_n) - f_n\|_{0,\Gamma},$$

$$e_r(\phi) = \frac{e(\phi)}{\|\phi\|_{0,\Gamma}}, e_r(\nabla_n \phi) = \frac{e(\nabla_n \phi)}{\|\nabla_n \phi\|_{0,\Gamma}}, e_r(f_n) = \frac{e(f_n)}{\|f_n\|_{0,\Gamma}}.$$

4.0.1. Born ion

The potential field (42) is exact for Born ion so our enriched gradient recovery method will give result with machine error, for that $1/|\mathbf{x} - \mathbf{x}_i|$ is one of the basis function of \mathbb{Q}_2 . For comparison, we present in Table (1) the errors in surface potential and gradients generated by PPR. It is seen that PPR has proved optimal rate of convergence and can give fairly good results when the mesh is sufficiently refined. In particular, a mesh space smaller than 0.1\AA is needed to generate a surface potential gradient with a relative error less than 10%, an accuracy barely sufficient for the real biomolecular simulations. The surface potential and magnitude of the surface gradient recovered using PPR at $h = 0.4\text{\AA}$ are shown in Fig. 2.

h	$e(\phi)$	$e_r(\phi)$	$e(\nabla \phi)$	$e_r(\nabla \phi)$
0.4	1.33	9.95e-2	7.97	1.18
0.2	2.10e-1	1.45e-2	3.02	2.58e-1
0.1	4.15e-2	2.83e-3	1.05	7.69e-2
0.05	6.69e-3	4.55e-4	3.16e-1	2.19e-2

Table 1: Errors and relative errors in surface potential and gradient recovered using PPR from the potential field (42) in Ω_s for Born ion.

4.0.2. Diatomic model

Our diatomic model consists of two unit spheres centered respectively at $(\pm 1, 0, 0)$, each carrying a unit positive charge at its center. We first set an analytical potential field (42) in Ω_s and recover the potential and potential gradient on surface using PPR and enriched recovery. If both charges are

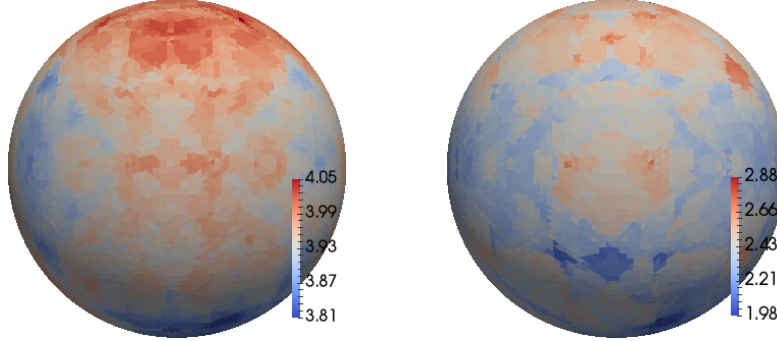


Figure 2: Surface potential (left; exact value 4.15 uniform) and magnitude of the surface gradient (right; exact value 4.15 uniform) recovered using PPR for Born ion. Mesh size $h = 0.4\text{\AA}$.

included for enrichment then recovered results will be accurate with machine error. Instead we choose the charge nearest to a surface point for the recovery there. It is seen from Table (2) that the enrichment with a single Green's function significantly improves the accuracy of the gradient recovery. At $h = 0.4\text{\AA}$, the relative error in surface gradient from enriched recovery is less than 8% while the traditional PPR method gives a surface gradient with an relative error more than 80%. This significant difference is also highlighted in Fig. 3, where a smoother and symmetric surface gradient is delivered by the enriched recovery.

h	PPR				Enriched Recovery			
	$e(\phi)$	$e_r(\phi)$	$e(\nabla\phi)$	$e_r(\nabla\phi)$	$e(\phi)$	$e_r(\phi)$	$e(\nabla\phi)$	$e_r(\nabla\phi)$
0.4	1.35	4.80e-2	9.60	8.17e-1	1.91e-1	6.44e-3	1.46	7.78e-2
0.2	2.77e-1	9.51e-3	3.98	2.31e-1	1.73e-2	5.82e-4	2.68e-1	1.24e-2
0.1	5.57e-2	1.90e-3	1.39	7.08e-2	3.49e-3	1.18e-4	8.90e-2	4.13e-3
0.05	9.12e-3	3.11e-4	4.23e-1	2.06e-2	5.48e-4	1.85e-5	2.69e-2	1.25e-3

Table 2: Errors and relative errors in surface potential and gradient recovered using PPR and enriched recovery from the potential field (42) in Ω_s for the diatomic molecule. The nearest atom is used in the enrichment.

The enriched recovery is also tested and compared to PPR on the numerical solutions of the PBE for this diatomic molecule. Since there does not exist analytical values of the surface potential and potential gradient, we would use

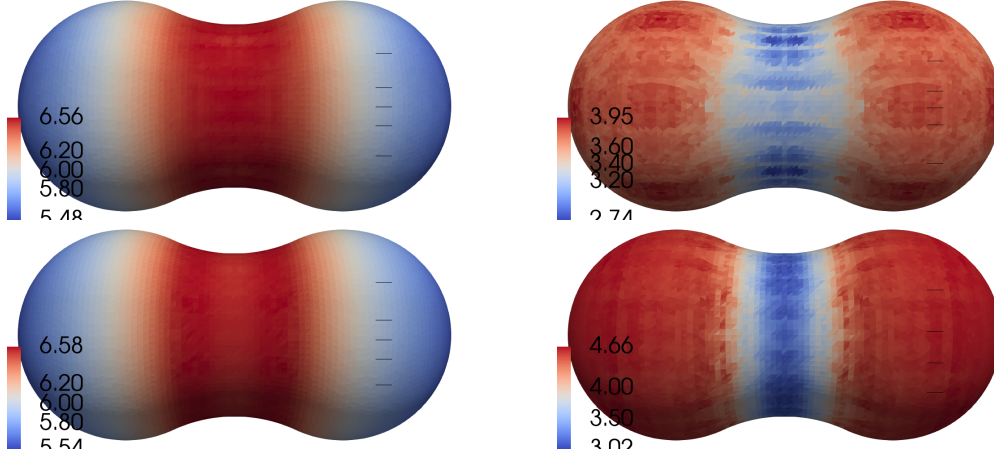


Figure 3: Surface potential (left) and magnitude of the surface gradient (right) recovered from the potential field (42) in Ω_s for diatomic molecule using PPR (top row) and enriched recovery (bottom). The nearest atom is used in the enrichment. Mesh size $h = 0.2\text{\AA}$.

the results of the enriched recovery at a fine mesh as the reference solution for error measurement. Both atoms are used in the enrichment for optimal recovery. The improvement of the accuracy in the recovered variables due to the enrichment is evidenced by the results collected in Table 3. This table and the plots in Fig. 4 show that both the PPR and enriched recovery can deliver accurate surface potential (top row) from the numerical solutions of the PBE but the accuracies of recovered gradients differ significantly. For all mesh sizes we tested the enriched recovery generates surface gradients with a consistent range. In contrast, the results of PPR vary considerably as the mesh is refined. At a fine mesh with $h = 0.05\text{\AA}$, notable variation is still observed in the surface gradient at the center neck of this diatomic molecule. The coupled enriched recovery is also tested on the numerical solutions of the PBE and the results are rather similar to the recovery based on the solution in Ω_s only.

4.0.3. Amino Acids

The numerical experiments above show that the accuracy of recovered gradients can be increased by enriching Green's functions at all charged atoms. For real biomolecular simulations we might not be able to afford this global enrichment because of the increasing computational cost. Global

h	PPR				Enriched Recovery			
	$e(\phi)$	$e_r(\phi)$	$e(\nabla\phi)$	$e_r(\nabla\phi)$	$e(\phi)$	$e_r(\phi)$	$e(\nabla\phi)$	$e_r(\nabla\phi)$
0.4	5.46e-1	1.86e-2	9.51	7.72e-1	8.23e-1	3.43e-2	1.08	7.22e-2
0.2	1.86e-1	6.32e-3	4.37	2.53e-1	2.76e-1	9.54e-3	4.72e-1	2.05e-2
0.1	5.71e-2	1.94e-3	1.54	7.74e-2	2.97e-2	9.89e-4	2.09e-1	9.18e-3
0.05	9.76e-3	3.31e-4	4.58e-1	2.20e-2				

Table 3: Errors and relative errors in surface potential and gradient recovered using PPR and enriched recovery from the numerical solutions of the PBE for solvated diatomic molecule. Both atoms are used in the enrichment. Errors are measured using the enriched recovery at $h = 0.05\text{\AA}$ as the reference solutions.

enrichment might not be necessary because the Green’s functions decay in $1/r$, which indicates the potential is prone to be dominated by the charges nearby. It is therefore possible only to choose a small set of charged atoms close to the surface point of recovery. Here we will test the enriched recovery on six amino acids: TRY, ASN, ASP, ARG, LYS and GLU dimer. For each amino acid, we set an analytical potential field using (42) assuming a unit positive charge at each atom.

As seen in Tables (4,5), the classical PPR ($m = 0$) has to use a very fine mesh $h = 0.05\text{\AA}$ to generate a surface gradient with a relative error about 2%. Recovery enriched with Green’s functions at 5 nearest atoms is able to deliver results of the similar accuracy at $h = 0.4\text{\AA}$. This number is also identified on the results for other residues, which are neglected as they show the very similar behavior as in these two tables. Enrichment with more Green’s functions will further improve the accuracy of the recovery but for the cause of efficiency we will choose $m = 5$ in the numerical experiments below.

We shall also compare PPR with enriched recovery on numerical solutions of the PBE for these amino acids. The surface potential and gradients recovered with the global enrichment at $h = 0.05\text{\AA}$ are taken as the reference solutions to examine the accuracy of recovery scheme enriched with different number of Green’s function and different h . The plots for ARG in Fig. 5 and for GLU dimer in Fig. 6 show that surface potential recovered by the classical PPR has an error more than 10% with respect to enriched recovery on a coarse mesh with $h = 0.4\text{\AA}$; the surface gradient delivered by PPR is indeed errant on the central neck of the GLU dimer. Despite the salient

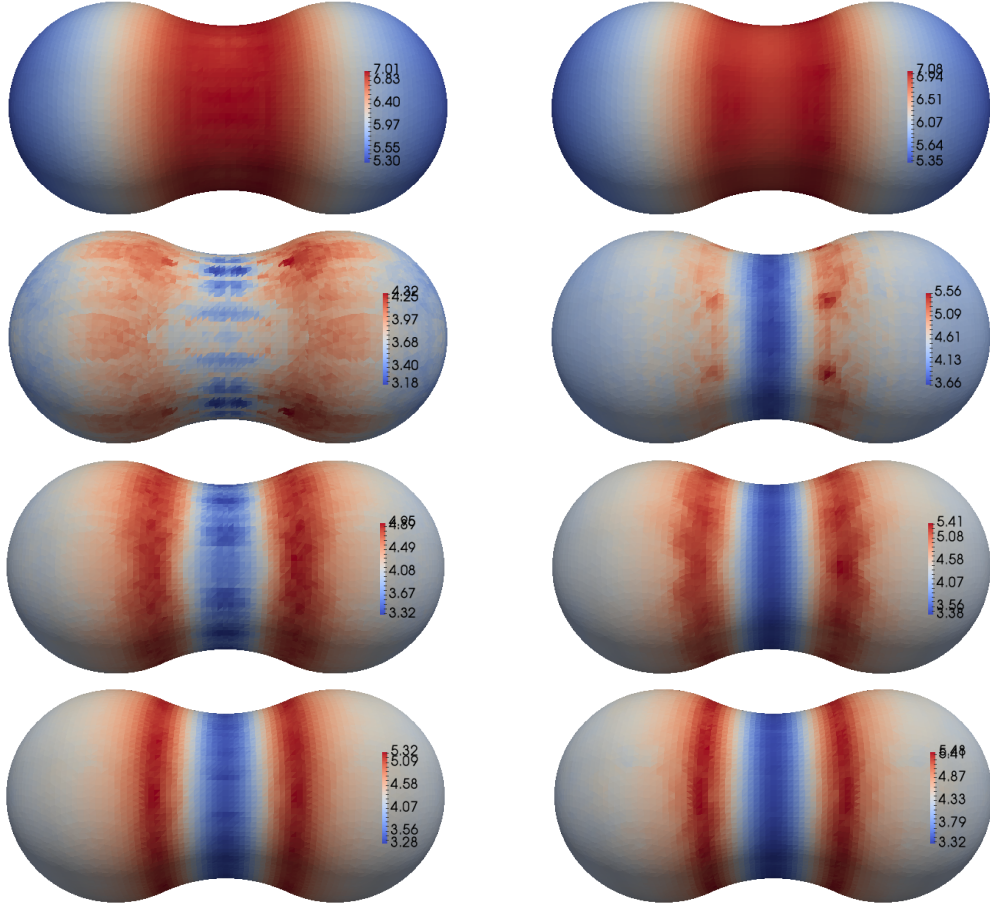


Figure 4: Surface potential (top row) and surface gradient (rest) recovered using PPR (left) and enriched recovery (right) from the numerical solutions of the PBE for solvated diatomic molecule. Both atoms are used in the enrichment. Mesh size $h = 0.2, 0.2, 0.1$ and 0.05 \AA from top to bottom.

errors in the surface quantities recovered by PPR on coarse meshes, these results converge to the same limit as the enriched recovery when the mesh of the numerical solutions for the PBE is sufficiently refined. In contrast, the enriched recovery produces very consistent surface potentials and surface gradients on all meshes tested, c.f., the ranges of these surface quantities in these plots.

m	$h = 0.4$		$h = 0.2$		$h = 0.05$	
	$e_r(\phi)$	$e_r(\nabla\phi)$	$e_r(\phi)$	$e_r(\nabla\phi)$	$e_r(\phi)$	$e_r(\nabla\phi)$
0	1.16e-1	8.00e-1	2.53e-2	2.46e-1	7.12e-4	2.10e-2
1	3.66e-2	1.62e-1	7.06e-3	5.68e-2	1.86e-4	5.49e-3
3	1.05e-2	4.35e-2	1.41e-3	1.17e-2	3.87e-5	1.17e-3
5	5.20e-3	2.22e-2	6.87e-4	5.44e-3	2.00e-5	5.71e-4
8	2.28e-3	9.67e-3	1.81e-4	1.47e-3	2.02e-5	5.19e-4
11	8.80e-4	3.62e-3	5.90e-5	4.99e-4	5.70e-6	1.39e-4
15	3.13e-4	1.35e-3	1.49e-5	1.23e-4	1.08e-6	2.84e-5
20	1.70e-5	9.04e-5	5.80e-7	5.17e-6	5.25e-7	1.32e-5

Table 4: Relative errors in the potential and gradient obtained from recovery enriched with different number of Green’s functions m for TYR surface. Exact potential field (42) is used. TYR consists of 21 atoms.

m	$h = 0.4$		$h = 0.2$		$h = 0.05$	
	$e_r(\phi)$	$e_r(\nabla\phi)$	$e_r(\phi)$	$e_r(\nabla\phi)$	$e_r(\phi)$	$e_r(\nabla\phi)$
0	1.05e-1	7.89e-1	2.34e-2	2.45e-1	6.56e-4	2.09e-2
1	3.94e-2	1.79e-1	8.25e-3	6.94e-2	2.07e-4	6.44e-3
3	1.12e-2	4.86e-2	1.88e-3	1.50e-2	3.63e-5	1.16e-3
5	5.20e-3	2.22e-2	6.85e-4	5.57e-3	1.41e-5	4.28e-4
7	2.56e-3	1.11e-2	4.27e-4	3.19e-3	2.02e-5	5.97e-4
9	1.09e-3	4.72e-3	1.34e-4	9.83e-4	1.03e-5	2.89e-4
12	1.80e-4	8.52e-4	1.73e-5	1.38e-4	2.26e-6	6.23e-5

Table 5: Relative errors in the potential and gradient obtained from recovery enriched with different number of Green’s functions m for ASN surface. Exact potential field (42) is used. ASN consists of 14 atoms.

4.0.4. Proteins

Our last numerical experiments are on a low-density lipoprotein receptor 1AJJ which has 37 residues and 519 atoms. The accuracy of the recovered surface potential and gradient from the numerical solutions of the PBE is documented in Tab. 6, where the results of the enriched recovery on the uniform mesh with $h = 0.05\text{\AA}$ is used as the reference. This table provides evidence of the higher accuracy of the enriched recovery over the classical PPR. For $h = 0.4\text{\AA}$, a relative error over 40% is found in the surface gradient

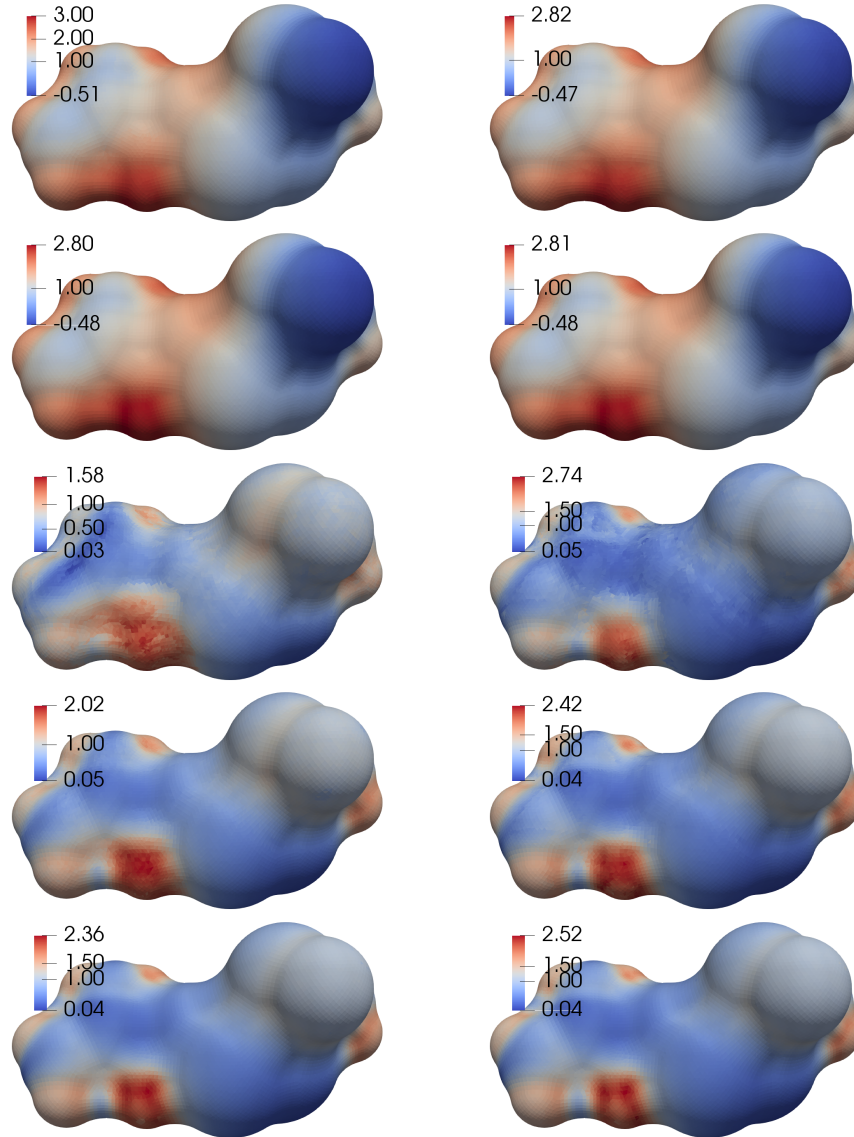


Figure 5: Surface potential (top two rows) and magnitude of the surface gradient (others) recovered using PPR (left) and enriched recovery (right) from the numerical solutions of the PBE for amino acid ARG. Five closest charged atoms are used in the enrichment. Mesh size $h = 0.4, 0.1, 0.4, 0.2$ and 0.1\AA from top to bottom.

recovered by PPR. This error is reduced to about 4% on a very fine mesh with

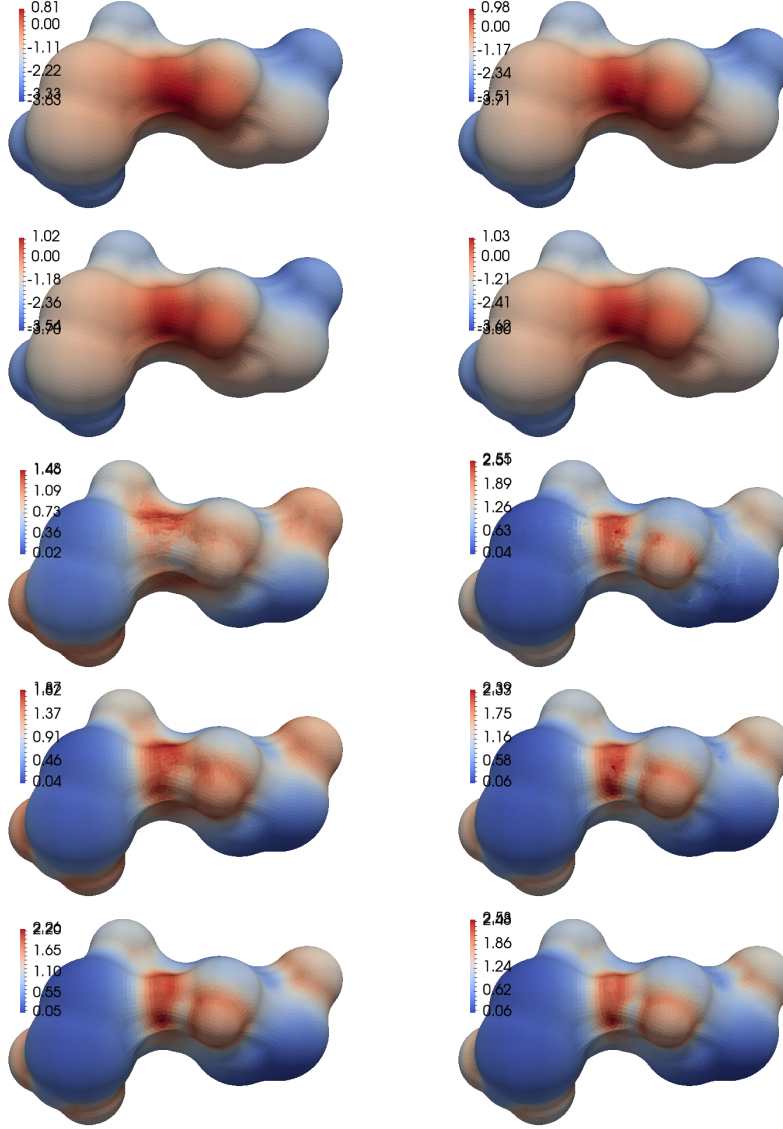


Figure 6: Surface potential (top two rows) and magnitude of the surface gradient (others) recovered using PPR (left) and enriched recovery (right) from the numerical solutions of the PBE for a GLU dimer. Five closest charged atoms are used in the enrichment. Mesh size $h = 0.4, 0.1, 0.4, 0.2$ and 0.1 \AA from top to bottom.

$h = 0.1 \text{ \AA}$, which is still larger than the enriched recovery on a coarse mesh

with $h = 0.4\text{\AA}$. The accuracy improvement due to the enrichment is also indicated in Fig. 7. Consistent with the observations on model molecules and amino acids above, enriched recovery produces more stable ranges of surface potential and gradient than PPR.

h	PPR				Enriched Recovery			
	$e(\phi)$	$e_r(\phi)$	$e(\nabla\phi)$	$e_r(\nabla\phi)$	$e(\phi)$	$e_r(\phi)$	$e(\nabla\phi)$	$e_r(\nabla\phi)$
0.4	1.61	1.87e-2	11.0	4.65e-1	1.52e-1	1.76e-3	9.49e-1	3.03e-2
0.2	3.59e-1	4.15e-3	4.50	1.60e-1	1.73e-2	2.00e-4	2.18e-1	6.96e-3
0.1	6.31e-2	7.30e-4	1.48	4.90e-2	2.70e-3	3.13e-5	6.28e-2	2.01e-3

Table 6: Errors and relative errors in surface potential and gradient recovered using PPR and enriched recovery from the numerical solutions of the PBE for solvated protein (PDB ID: 1AJJ). At most five closest charged atoms within a distance of 8\AA are used in the enrichment.

5. Concluding Remarks

We present in this paper a novel numerical method for computing the potential and its gradient on the molecular surfaces from the numerical solutions of the Poisson-Boltzmann equation, which is widely used in modeling the electrostatic interactions for biomolecules in solvent. Our method reconstructs a solution in the least square sense locally in the solvent region. In contrast to the classical polynomial preserving recovery (PPR) method that is based only on the polynomial basis functions, our reconstruction enriches the basis with Green’s functions modeling the electrostatic potential field induced by selected charges. This enrichment is motivated by the Generalized Born method which decomposes the electrostatic potential inside the solute molecules into a Coulomb potential and a reaction field, and also by the approximate boundary condition for the Poisson-Boltzmann equation. Extensive numerical methods on Born atom, model diatomic molecule, amino acids, and proteins demonstrate that our enriched recovery is more accurate than PPR on the same mesh, more stable along the mesh refinement, and indeed provides a stable reference to which the PPR solutions will converge.

Our enriched recovery is easy to implement, and can be readily integrated with other interface finite difference or finite element methods for the

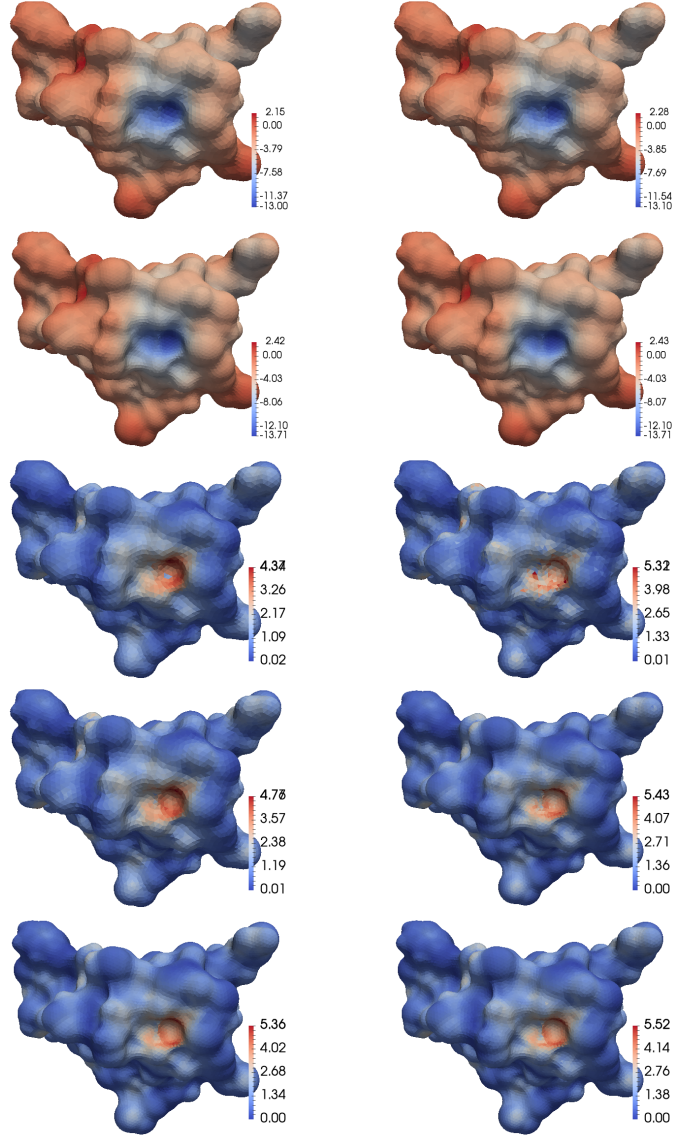


Figure 7: Surface potential (top two rows) and magnitude of the surface gradient (others) recovered using PPR (left) and enriched recovery (right) from the numerical solutions of the PBE for solvated protein (PDB ID: 1AJJ). At most five closest charged atoms with a distance of 8\AA are used in the enrichment. Mesh size $h = 0.4, 0.1, 0.4, 0.2$ and 0.1\AA from top to bottom.

Poisson-Boltzmann equation. As the reconstruction is independently computed at each surface point of interest, parallelization of this enriched recovery is straightforward. We are currently working to supply the recovered surface gradient to compute the dielectric boundary force and use the force to drive the large scale continuum molecular deformation as induced due to varying solvation states such as binding of molecules or ligands, changes in ion concentration, or protonation.

Acknowledgements

This work has been partially supported by National Institutes of Health through the grant R01GM117593 as part of the joint DMS/NIGMS initiative to support research at the interface of the biological and mathematical sciences.

References

- [1] B. Honig, A. Nicholls, Classical electrostatics in biology and chemistry, *Science* 268 (5214) (1995) 1144–1149. doi:10.1126/science.7761829.
- [2] W. Im, D. Beglov, B. Roux, Continuum solvation model: Computation of electrostatic forces from numerical solutions to the Poisson-Boltzmann equation, *Comput. Phys. Commun.* 111 (1998) 59–75. doi:10.1016/S0010-4655(98)00016-2.
- [3] B. Lu, Y. C. Zhou, M. Holst, J. A. McCammon, Recent progress in numerical solution of the Poisson-Boltzmann equation for biophysical applications, *Commun. Comput. Phys.* 3 (2008) 973–1009.
- [4] P. Ren, J. Chun, D. G. Thomas, M. J. Schnieders, M. Marucho, J. Zhang, N. A. Baker, Biomolecular electrostatics and solvation: a computational perspective 45 (2012) 427–491. doi:10.1017/S003358351200011X.
- [5] D. Xie, Y. Jiang, L. R. Scott, Efficient algorithms for a nonlocal dielectric model for protein in ionic solvent, *SIAM J. Sci. Comput.* 35 (2013) 1267–1284. doi:10.1137/120899078.
- [6] J. Chen, W. Geng, On preconditioning the treecode-accelerated boundary integral (tabi) Poisson-Boltzmann solver, *J. Comput. Phys.* 373 (2018) 750–762. doi:10.1016/j.jcp.2018.07.011.

- [7] Y. Zhong, K. Ren, R. Tsai, An implicit boundary integral method for computing electric potential of macromolecules in solvent, *J. Comput. Phys.* 359 (2018) 199 – 215. doi:10.1016/j.jcp.2018.01.021.
- [8] A. D. MacKerell, D. Bashford, M. Bellott, R. L. Dunbrack, J. D. Evanseck, M. J. Field, S. Fischer, J. Gao, H. Guo, S. Ha, D. Joseph-McCarthy, L. Kuchnir, K. Kuczera, F. T. K. Lau, C. Mattos, S. Michnick, T. Ngo, D. T. Nguyen, B. Prodhom, W. E. Reiher, B. Roux, M. Schlenkrich, J. C. Smith, R. Stote, J. Straub, M. Watanabe, J. Wirkiewicz-Kuczera, D. Yin, M. Karplus, All-atom empirical potential for molecular modeling and dynamics studies of proteins, *J. Phys. Chem. B* 102 (18) (1998) 3586–3616. arXiv:<https://doi.org/10.1021/jp973084f>, doi:10.1021/jp973084f.
- [9] Q. Lu, R. Luo, A Poisson-Boltzmann dynamics method with nonperiodic boundary condition, *J. Chem. Phys.* 119 (21) (2003) 11035–11047.
- [10] N. V. Prabhu, P. J. Zhu, K. A. Sharp, Implementation and testing of stable, fast implicit solvation in molecular dynamics using the smooth-permittivity finite difference Poisson-Boltzmann method, *J. Comput. Chem.* 25 (16) (2004) 2049–2064. doi:10.1002/jcc.20138.
- [11] W. Geng, G. W. Wei, Multiscale molecular dynamics using the matched interface and boundary method, *J. Comput. Phys.* 230 (2011) 435–457. doi:10.1016/j.jcp.2010.09.031.
- [12] Y. Tang, G. Cao, X. Chen, J. Yoo, A. Yethiraj, Q. Cui, A finite element framework for studying the mechanical response of macromolecules: application to the gating of mechanosensitive channel MscL, *Biophys. J.* 91 (2006) 1248–1263. doi:10.1529/biophysj.106.085985.
- [13] L. Ma, A. Yethiraj, X. Chen, Q. Cui, A computational framework for mechanical response of macromolecules: applications to the salt concentration dependence of DNA bendability, *Biophys. J.* 96 (2009) 3542–3554.
- [14] X. Chen, Q. Cui, Computational molecular biomechanics: A hierarchical multiscale framework with applications to gating of mechanosensitive channels of large conductance, in: T. Dumitrica (Ed.), *Trends in Computational Nanomechanics*, Vol. 9 of *Challenges and Advances in*

Computational Chemistry and Physics, Springer Netherlands, 2010, pp. 535–556.

- [15] Y. C. Zhou, B. Lu, A. A. Gorfe, Continuum electromechanical modeling of protein-membrane interactions, *Phys. Rev. E* 82 (4) (2010) 041923. doi:10.1103/PhysRevE.82.041923.
- [16] L.-T. Cheng, B. Li, M. White, S. Zhou, Motion of a cylindrical dielectric boundary, *SIAM J. Appl. Math.* 73 (2013) 594–616. doi:10.1137/120867986.
- [17] M. K. Gilson, M. E. Davis, B. A. Luty, J. A. McCammon, Computation of electrostatic forces on solvated molecules using the Poisson-Boltzmann equation, *J. Phys. Chem.* 97 (14) (1993) 3591–3600. doi:10.1021/j100116a025.
- [18] Y. Zhou, M. Holst, J. A. McCammon, Nonlinear elastic modeling of macromolecular conformational change induced by electrostatic forces, *J. Math. Anal. Appl.* 340 (2008) 135–164. doi:10.1016/j.jmaa.2007.07.084.
- [19] B. Li, X. Cheng, Z. Zhou, Dielectric boundary force in molecular solvation with the Poisson-Boltzmann free energy: A shape derivative approach, *SIAM J. Appl. Math.* 71 (2011) 2093–2111. doi:10.1137/110826436.
- [20] M. Mikucki, Y. C. Zhou, Electrostatic forces on charged surfaces of bilayer lipid membranes, *SIAM J. Appl. Math.* 74 (2014) 1–21. doi:10.1137/130904600.
- [21] J. Frank H. Stillinger, Interfacial solutions of the poisson-boltzmann equation, *J. Chem. Phys.* 35 (5) (1961) 1584–1589. doi:10.1063/1.1732113.
- [22] Z. X. Xiang, Y. Y. Shi, Y. W. Xu, Solving the finite-difference, nonlinear, Poisson-Boltzmann equation under a linear-approach, *J. Comput. Chem.* 16 (2) (1995) 200–206. doi:10.1002/jcc.540160207.
- [23] M. Holst, F. Saied, Numerical solution of the nonlinear Poisson-Boltzmann equation: Developing more robust and efficient methods., *J. Comput. Chem.* 16 (1995) 337–364. doi:10.1002/jcc.540160308.

- [24] M. Holst, N. A. Baker, F. Wang, Adaptive multilevel finite element solution of the Poisson-Boltzmann equation I: algorithms and examples, *J. Comput. Chem.* 21 (2000) 1319–1342.
- [25] A. H. Boschitsch, M. O. Fenley, H.-X. Zhou, Fast boundary element method for the linear Poisson-Boltzmann equation, *J. Phys. Chem. B* 106 (10) (2002) 2741–2754. doi:10.1021/jp013607q.
- [26] D. Xie, S. Zhou, A new minimization protocol for solving nonlinear Poisson-Boltzmann mortar finite element equation, *BIT* 47 (2007) 853–871, in press. doi:10.1007/s10543-007-0145-9.
- [27] H. Lin, H. Tang, W. Cai, Accuracy and efficiency in computing electrostatic potential for an ion channel model in layered dielectric/electrolyte media, *J. Comput. Phys.* 259 (2014) 488 – 512. doi:10.1016/j.jcp.2013.12.017.
- [28] W. Geng, S. Zhao, A two-component matched interface and boundary (MIB) regularization for charge singularity in implicit solvation, *J. Comput. Phys.* 351 (2017) 25 – 39. doi:10.1016/j.jcp.2017.09.026.
- [29] B. Z. Lu, X. L. Cheng, J. F. Huang, J. A. McCammon, Order N algorithm for computation of electrostatic interactions in biomolecular systems, *Proc. Natl. Acad. Sci. U. S. A.* 103 (51) (2006) 19314–19319. doi:10.1073/pnas.0605166103.
- [30] C. Bajaj, S. Chen, A. Rand, An efficient higher-order fast multipole boundary element solution for Poisson-Boltzmann-based molecular electrostatics, *SIAM J. Sci. Comput.* 33 (2) (2011) 826–848. doi:10.1137/090764645.
- [31] W. Geng, R. Krasny, A treecode-accelerated boundary integral Poisson-Boltzmann solver for electrostatics of solvated biomolecules, *J. Comput. Phys.* 247 (2013) 62–78. doi:10.1016/j.jcp.2013.03.056.
- [32] H. Guo, X. Yang, Gradient recovery for elliptic interface problem: I. body-fitted mesh, *Commun. Comput. Phys.* 23 (2018) 1488–1511. doi:10.4208/cicp.0A-2017-0026.

- [33] H. Guo, X. Yang, Gradient recovery for elliptic interface problem: II. immersed finite element methods, *J. Comput. Phys.* 338 (2017) 606 – 619. doi:10.1016/j.jcp.2017.03.003.
- [34] H. Guo, X. Yang, Gradient recovery for elliptic interface problem: III. Nitsche’s method, *J. Comput. Phys.* 356 (2018) 46 – 63. doi:10.1016/j.jcp.2017.11.031.
- [35] O. C. Zienkiewicz, J. Z. Zhu, The superconvergent patch recovery and a posteriori error estimates. Part 1: The recovery technique, *Internat. J. Numer. Methods Eng.* 33 (1992) 1331–1364. doi:10.1002/nme.1620330702.
- [36] O. C. Zienkiewicz, J. Z. Zhu, The superconvergent patch recovery and a posteriori error estimates. Part 2: Error estimates and adaptivity, *Internat. J. Numer. Methods Eng.* 33 (1992) 1365–1382. doi:10.1002/nme.1620330703.
- [37] R. Bank, J. Xu, Asymptotically exact a posteriori error estimators, part ii: General unstructured grids, *SIAM J. Numer. Anal.* 41 (6) (2003) 2313–2332. doi:10.1137/S0036142901398751.
- [38] H. Guo, Z. Zhang, Gradient recovery for the Crouzeix–Raviart element, *J. Sci. Comput.* 64 (2) (2015) 456–476. doi:10.1007/s10915-014-9939-5.
- [39] A. Naga, Z. Zhang, The polynomial-preserving recovery for higher order finite element methods in 2D and 3D 5 (2005) 769–798. doi:10.3934/dcddb.2005.5.769.
- [40] J. Xu, Z. Zhang, Analysis of recovery type a posteriori error estimators for mildly structured grids, *Math. Comp.* 247 (2003) 1139–1152. doi:10.1090/S0025-5718-03-01600-4.
- [41] Z. Zhang, A. Naga, A new finite element gradient recovery method: Superconvergence property, *SIAM J. Sci. Comput.* 26 (4) (2005) 1192–1213. doi:10.1137/S1064827503402837.
- [42] S.-H. Chou, An immersed linear finite element method with interface flux capturing recovery 17 (2012) 2343. doi:10.3934/dcddb.2012.17.2343.

- [43] S.-H. Chou, C. Attanayake, Flux recovery and superconvergence of quadratic immersed interface finite elements, *Int. J. Numer. Anal. Mod.* 14 (2015) 88–102.
- [44] H. Wei, L. Chen, Y. Huang, B. Zheng, Adaptive mesh refinement and superconvergence for two-dimensional interface problems, *SIAM J. Sci. Comput.* 36 (4) (2014) A1478–A1499. doi:10.1137/120866622.
- [45] Z. Li, H. Ji, X. Chen, Accurate solution and gradient computation for elliptic interface problems with variable coefficients, *SIAM J. Numer. Anal.* 55 (2) (2017) 570–597. doi:10.1137/15M1040244.
- [46] Z. Li, The immersed interface method using a finite element formulation, *Appl. Numer. Math.* 27 (3) (1998) 253–267. doi:10.1016/S0168-9274(98)00015-4.
- [47] X.-D. Liu, R. P. Fedkiw, M. Kang, A boundary condition capturing method for poisson’s equation on irregular domains, *J. Comput. Phys.* 160 (1) (2000) 151–178. doi:10.1006/jcph.2000.6444.
- [48] S. Hou, P. Song, L. Wang, H. Zhao, A weak formulation for solving elliptic interface problems without body fitted grid, *J. Comput. Phys.* 249 (2013) 80 – 95. doi:10.1016/j.jcp.2013.04.025.
- [49] H. Ji, J. Chen, Z. Li, A symmetric and consistent immersed finite element method for interface problems, *J. Sci. Comput.* 61 (3) (2014) 533–557. doi:10.1007/s10915-014-9837-x.
- [50] P. Hansbo, Nitsche’s method for interface problems in computational mechanics, *GAMM - Mitteilungen* 28 (2005) 183–206. doi:10.1002/gamm.201490018.
- [51] C. Annavarapu, M. Hautefeuille, J. E. Dolbow, A robust Nitsche’s formulation for interface problems, *Comput. Methods Appl. Mech. Eng.* 225-228 (2012) 44–54. doi:https://doi.org/10.1016/j.cma.2012.03.008.
- [52] W. Im, M. S. Lee, C. L. B. III, Generalized Born model with a simple smoothing function, *J. Comput. Chem.* 24 (2003) 1691–1702. doi:10.1002/jcc.10321.

- [53] M. Feig, W. Im, C. L. B. III, Implicit solvation based on generalized Born theory in different dielectric environments, *J. Comput. Chem.* 120 (2004) 903–911. doi:10.1063/1.1631258.
- [54] A. V. Onufriev, D. A. Case, Generalized Born implicit solvent models for biomolecules, *Annu. Rev. Biophys.* 48 (2019) 275–296. doi:10.1146/annurev-biophys-052118-115325.
- [55] M. K. Gilson, A. Rashin, R. Fine, B. Honig, On the calculation of electrostatic interactions in proteins, *J. Mol. Biol.* 184 (3) (1985) 503–516. doi:10.1016/0022-2836(85)90297-9.
- [56] K. A. Sharp, B. Honig, Calculating total electrostatic energies with the nonlinear Poisson-Boltzmann equation, *J. Phys. Chem.* 94 (19) (1990) 7684–7692. doi:10.1021/j100382a068.
- [57] K. A. Sharp, B. Honig, Electrostatic interactions in macromolecules - theory and applications, *Annu. Rev. Biophys. Biophys. Chem.* 19 (1990) 301–332. doi:10.1146/annurev.bb.19.060190.001505.
- [58] L. Chen, M. Holst, J. Xu, The finite element approximation of the nonlinear Poisson-Boltzmann equation, *SIAM J. Numer. Anal.* 45 (2007) 2298–2320. doi:10.1137/060675514.
- [59] M. Holst, J. A. McCammon, Z. Yu, Y. C. Zhou, Y. Zhu, Adaptive finite element modeling techniques for the Poisson-Boltzmann equation, *Commun. Comput. Phys.* 11 (2012) 179–214. doi:10.4208/cicp.081009.130611a.
- [60] I.-L. Chern, J.-G. Liu, W.-C. Wang, Accurate evaluation of electrostatics for macromolecules in solution, *Methods Appl. Anal.* 10 (2003) 309–328.
- [61] Y. C. Zhou, B. Z. Lu, G. A. Huber, M. J. Holst, J. A. McCammon, Continuum simulations of acetylcholine consumption by acetylcholinesterase - a Poisson-Nernst-Planck approach, *J. Phys. Chem. B* 112 (2) (2008) 270–275.
- [62] B. Roux, H.-A. Yu, M. Karplus, Molecular basis for the Born model of ion solvation, *J. Phys. Chem.* 94 (1990) 4683–4688. doi:10.1021/j100374a057.

- [63] Y. C. Zhou, S. Zhao, M. Feig, G. W. Wei, High order matched interface and boundary (MIB) schemes for elliptic equations with discontinuous coefficients and singular sources, *J. Comput. Phys.* 213 (2006) 1–30.
- [64] W. Geng, S. Yu, G. Wei, Treatment of charge singularities in implicit solvent models, *J. Chem. Phys.* 127 (2007) 114106.